Mechanical Properties and Elastic Behavior of High-Molecular-Weight Poorly Syndiotactic Polypropylene

Claudio De Rosa,* Finizia Auriemma, and Odda Ruiz de Ballesteros

Dipartimento di Chimica, Università di Napoli "Federico II", Complesso Monte S. Angelo, Via Cintia, 80126 Napoli, Italy

Received June 18, 2003; Revised Manuscript Received July 21, 2003

ABSTRACT: An analysis of the mechanical properties and elastic behavior of low-stereoregular and nearly amorphous syndiotactic polypropylene (*sam*-PP), prepared with heterocycle-fused indenyl silyl amido dimethyltitanium complexes, is presented. High-molecular-weight poorly syndiotactic *sam*-PP samples show good elastic behavior at room temperature in a large range of deformation. While highly stereoregular and crystalline syndiotactic polypropylene shows good elastic properties only for previously stretched oriented fibers, *sam*-PP samples present good elasticity even for unoriented compression-molded films during the first stretching. Because of the very low crystallinity, these samples experience a negligible irreversible plastic deformation and show a typical behavior of thermoplastic elastomers. The small crystalline domains in the amorphous matrix act as physical knots of the elastomeric lattice, preventing the viscous flow of the amorphous chains. The elastic behavior is associated with a reversible polymorphic transition between the *trans*-planar mesomorphic form and helical form I, which occurs in the crystalline domains during successive stretching and relaxing of fiber specimens, giving an enthalpic contribution which assists the elastic recovery of the samples. The entropic effect of the conformational transition of the amorphous chains, connecting the crystalline domains as tie chains, is, however, mainly responsible for the elasticity. The comparison with the mechanical properties of high-molecular-weight amorphous polypropylene samples has shown that the latter present lower strength and experience rapid viscous flow of the chains at high deformations and/or by application of stresses for long time. The presence of crystallinity in the *sam*-PP samples increases the strength, producing interesting thermoplastic elastomeric materials.

Introduction

In recent papers the synthesis and the structural characterization of poorly syndiotactic, nearly amorphous polypropylene (*sam*-PP) with high molecular weights have been described.[1,2] The polypropylene samples have been prepared with catalytic systems composed of silyl-bridged indenyl *tert*-butylamido complexes of titanium, in which the indenyl ligand has a heterocycle condensed onto the cyclopentadienyl moiety (**1** and **2** in Chart 1),[3] activated with methylaluminoxane (MAO). The polymer samples, prepared with **1**/MAO and **2**/MAO, are characterized by a prevailingly syndiotactic microstructure, with fully syndiotactic pentad contents [*rrrr*] in the range 40−55%. The microstructural and the physical properties of *sam*-PP samples have been compared with those of the fully amorphous polypropylene samples (*am*-PP), having lower syndiotacticity ([*rrrr*] = 26%),[1] prepared with the Dow catalyst dimethylsilyl tetramethylcyclopentadienyl *tert*-butylamido dichlorotitanium (catalyst **3** of Chart 1).[4]

As-prepared *sam*-PP samples are amorphous and do not crystallize by cooling the melt to room temperature but slowly crystallize if the samples are kept at room temperature for several days.[2] Maximum degrees of crystallinity in the range 16−20% are achieved.[1,2] *am*-PP samples prepared with **3**/MAO are amorphous and do not crystallize even for long aging time at room temperature.

The structural characterization of *sam*-PP samples has shown that the low stereoregularity strongly influences the polymorphic behavior of syndiotactic polypropylene (s-PP).[2] It is well-known that s-PP presents a complex polymorphism complicated by the presence of structural disorder.[5−22] Four crystalline forms,[5,6,10−17] and a mesomorphic form,[18,19] have been described. The most stable form I and the metastable form II are characterized by chains in the **s**(2/1)2 helical $(T_2G_2)_n$ conformation, packed in orthorhombic unit cells.[5,6,12−15] The two metastable modifications, form III and form IV, present chains in *trans*-planar[10] and $(T_6G_2T_2G_2)_n$[11,17] helical conformations, respectively. A polymorphic transition between *trans*-planar form III and isochiral helical form II has been observed in oriented fibers.[15] *trans*-Planar form III can be obtained by stretching at room temperature highly stereoregular s-PP samples[10,12] and transforms into isochiral helical form II upon release of the tension.[15,20] This solid-state transition is reversible; *trans*-planar form III and helical form II transform into each other by stretching and relaxing oriented fibers.[15,20,21]

A slightly different polymorphic behavior has been observed in low-stereoregular *sam*-PP samples.[2] These samples crystallize in disordered modifications of helical

Chart 1

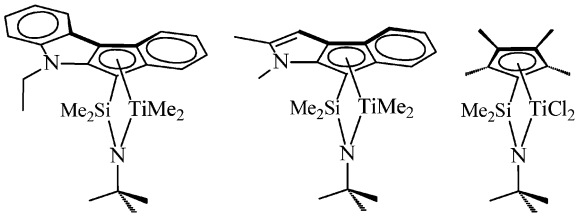

1 **2** **3**

* To whom correspondence should be addressed. Phone: ++39 081 674346. Fax: ++39 081 674090. E-mail: derosa@chemistry.unina.it.

10.1021/ma034829k CCC: $25.00 © 2003 American Chemical Society
Published on Web 09/12/2003

form I of s-PP.[1,2] Disorder in the alternation of right- and left-handed helical chains along the axes of the unit cell[14] and disorder in the stacking of *bc* layers of chains along *a*, implying shifts of *bc* layers of *b*/4 along *b*,[9,14] are present. The stretching of compression-molded films of *sam*-PP samples produces oriented crystalline fibers in the *trans*-planar mesomorphic form of s-PP.[2] The low stereoregularity prevents the formation of ordered *trans*-planar form III of s-PP, which instead is obtained in stretched fibers of the highly stereoregular and crystalline s-PP.[10,12] Upon release of the tension in stretched fibers of *sam*-PP samples, the *trans*-planar mesomorphic form transforms into helical form I.[2] Isochiral helical form II of s-PP, which is generally obtained in s-PP fibers initially in *trans*-planar form III by removing the tension,[15,20] has never been observed in *sam*-PP fiber samples. These data have confirmed that isochiral form II of s-PP can be obtained only starting from *trans*-planar form III through a spontaneous cooperative crystal−crystal transformation when the tension in stretched fibers is removed.[15,21,23,24]

The physical properties of s-PP strongly depend on the polymorphic behavior. For instance, oriented fibers of s-PP show elastic behavior,[20,21,25,26] which is related to the structural organization. Unoriented compression-molded samples of s-PP behave like a typical highly crystalline material showing a plastic deformation upon stretching at room temperature.[20,21,26] The crystalline domains, with chains in a helical conformation, tend to assume a preferred orientation along the stretching direction, causing a plastic, not reversible, deformation. High orientation of the crystalline phase is generally achieved. Along with this plastic deformation, a phase transition from the most stable helical form I into *trans*-planar form III gradually occurs.[20,21] The phase transition is reversible; after the tension is released, the crystalline domains remain nearly oriented with the *c* axis parallel to the preferred (stretching) direction, and *trans*-planar form III transforms again into the more stable helical form.[20,21] Correspondigly, only a partial recovery of the macroscopic dimensions of the sample is attained. Therefore, unoriented samples show only fair or poor elastic properties.[20,21,25,26]

Stress-relaxed fibers of s-PP show instead very good elastic behavior upon successive stretching and relaxation; the helical form transforms by stretching into the *trans*-planar form, which transforms again into the helical form upon release of the tension, and a nearly total recovery of the initial dimensions of the fiber samples is observed.[20,21,25,26] When the crystalline domains are already oriented along the stretching direction, that is, when the sample has already undergone the plastic deformation, the fibers show good elastic properties. Of course, during the mechanical cycles also the chains in the amorphous regions are subjected to a reversible conformational transition, from the "random coils" into extended conformations, and vice versa. The reversibility of this transition is possibly assisted and is, somehow, favored by the polymorphic transition occurring in the crystalline regions.

It has been suggested that both the metastability of *trans*-planar form III, which transforms into the stable helical form when the tension is relaxed,[20,21] and the conformational transition of the chains in the amorphous phase[21,25,26] play key roles in the elastic behavior of s-PP. The structural transition occurring in the crystalline regions, due to the metastability of *trans*-planar form in the unstrained state, produces an enthalpy gain when the tension is removed, which is in part responsible of the elastic recovery of the fibers.[20,21] On the other hand, chains belonging to the amorphous phase and connecting the crystalline regions as tie chains, are also involved in the stretching and relaxation process. These chains are probably well-oriented and highly entangled and in an extended conformation in the stretched state, and experience a reversible conformational transition between disordered (coil) and extended conformations when the fibers are repeatedly stretched and relaxed. This entropic factor is probably also involved in the recovery process.[21,26] The two effects, the enthalpy gain in the crystalline regions and the entropic factor of the amorphous chains, act simultaneously and are, probably, mutually assisted. However, the relative weight of these two effects is still not completely clarified.

In this paper the mechanical properties and the elastic behavior of high-molecular-weight, low-crystalline *sam*-PP samples are analyzed and compared to the mechanical properties of highly syndiotactic polypropylene, prepared with C_s-symmetric catalysts, and high-molecular-weight amorphous polypropylene prepared with the Dow catalyst **3**. The study of the polymorphic behavior and mechanical properties of these poorly syndiotactic polypropylene samples may give new insights into the relationship between the elastic behavior and the structural organization of s-PP. Since *sam*-PP samples present high molecular weights and very low crystallinity, they provide a unique opportunity to analyze whether the outstanding mechanical properties of s-PP are really linked to the crystal structure of fiber specimens and to the structural transition occurring in the crystalline phase. Since for *sam*-PP samples the formation of *trans*-planar form III by stretching is prevented,[2] the enthalpic contribution to the elasticity is probably reduced.[20] On the other hand, the lower crystallinity should produce an increase of the entropic contribution due to the increased fraction of tie chains connecting the smaller crystalline domains.

Experimental Section

Poorly syndiotactic *sam*-PP samples were provided by Dr. Luigi Resconi of Basell Polyolefins (Ferrara, Italy). The samples were prepared using catalysts **1** and **2** (Chart 1) activated with MAO, whereas fully amorphous polypropylene *am*-PP samples were prepared with catalyst **3** (Chart 1), as described in ref 1. The intrinsic viscosities, the molecular weights, the melting temperatures, and the microstructural characteristic (distribution of pentad stereosequences) are reported in Table 1. The NMR analysis indicates that *sam*-PP samples prepared with **1**/MAO and **2**/MAO are prevailingly syndiotactic, with fully syndiotactic pentad contents [*rrrr*] in the range 40−55%, whereas *am*-PP samples, prepared with **3**/MAO, show lower values of the syndiotactic pentad contents (nearly 26%).

X-ray diffraction patterns were obtained with Ni-filtered Cu Kα radiation. The powder profiles were obtained with an automatic Philips diffractometer, whereas the fiber diffraction patterns were recorded on a BAS-MS imaging plate (FUJIFILM) using a cylindrical camera and processed with a digital imaging reader (FUJIBAS 1800). The X-ray fiber diffraction patterns were recorded for stretched fibers soon after the stretching and keeping the fiber under tension, as well as for relaxed fibers, that is, after the fiber was kept under tension for 10 min and then the tension was removed, allowing the complete relaxation of the specimens. The X-ray diffraction pattern of the amorphous phase was subtracted from all the fiber diffraction patterns.

Table 1. Polymerization Temperatures (T_p), Intrinsic Viscosities (IV), Molecular Weights (M_w), Melting Temperatures (T_m), and Contents of Pentad and Diad Stereosequences (%) of *sam*-PP Samples Prepared with Catalysts 1/MAO and 2/MAO and *am*-PP Samples Prepared with Catalyst 3/MAO

sample	T_p (°C)	catalyst	IV (dL/ g)	M_w	T_m[b] (°C)	[*mmmm*]	[*mmmr*]	[*rmmr*]	[*mmrr*]	[*xmrx*]	[*rmrm*]	[*rrrr*]	[*rrrm*]	[*mrrm*]	[*m*]	[*r*]
*sam*PP1	70	**1**	5.96	1308600	59	0.31	1.75	2.90	8.81	10.32	2.38	54.62	16.31	2.59	15.73	84.27
*sam*PP2	60	**2**	3.65	672700	50	0.00	1.36	2.91	7.05	13.69	2.83	51.60	17.52	3.04	16.06	83.94
*sam*PP3	80	**2**[a]	5.43	1153200	48	0.53	2.01	3.24	7.73	14.81	3.84	45.84	18.64	3.36	18.97	81.03
*sam*PP4	80	**2**[a]	4.47	885700	48	0.27	2.14	3.39	7.55	13.76	3.66	46.86	18.02	4.35	18.29	81.72
*sam*PP5	80	**2**[a]	3.31	589200	47	0.78	2.69	3.75	8.84	15.63	4.64	41.42	18.33	3.92	21.77	78.23
*am*PP6	50	**3**	5.56	1190800	-	0.76	3.53	5.24	9.96	19.53	8.60	26.52	19.57	6.29	28.57	71.43
*am*PP7	60	**3**	2.42	385200	-	0.95	3.56	5.24	10.23	20.14	8.75	25.73	19.56	5.84	29.31	70.69

[a] Samples *sam*-PP3, *sam*-PP4, and *sam*-PP5 were prepared with the catalyst **2**/MAO supported on polyethylene.[1] [b] Peak temperatures from DSC heating scans at 10 °C/min.

The melting temperatures of the semicrystalline samples were obtained with a differential scanning calorimeter (Perkin-Elmer DSC-7) performing scans in a flowing N_2 atmosphere and at a heating rate of 10 °C/min.

Mechanical tests were performed on compression-molded films, after complete crystallization was achieved at room temperature. Powder samples were melted between perfectly flat brass plates under a press at very low pressure, and slowly cooled to room temperature. Special care was taken to obtain films with uniform thickness (0.3 mm) and minimize surface roughness, according to the recommendation of the standard ASTM D2292-85. Films obtained by compression molding were kept at room temperature for at least one week before the tests, allowing the complete crystallization in the case of the crystallizable samples. The mechanical tests were performed at room temperature with a miniature mechanical tester apparatus (Minimat, by Rheometrics Scientific), following the standard test method for tensile properties of thin plastic sheeting, ASTM D882-83.

Mechanical tests were first performed on the unstretched compression-molded films. Rectangular specimens 10 mm long, 5 mm wide, and 0.3 mm thick were stretched up to the break or up to a given strain ϵ. Similar tests were then performed at room temperature on the strained and stress-relaxed fibers. Stress-relaxed fiber specimens were prepared by stretching the compression-molded films up to strains of 200% and 400%, keeping the fibers under tension for 10 min at room temperature, and then removing the tension, allowing the specimens to relax. The fibers of *sam*-PP samples stress-relaxed from 200% and 400% strain are identified as *sam*PP*n*-200 and *sam*PP*n*-400, respectively, with $n = 1-5$ corresponding to samples *sam*PP1−*sam*PP5 of Table 1. The fibers of *am*-PP samples stress-relaxed from 200% and 400% strain are identified as *am*PP*n*-200 and *am*PP*n*-400, respectively, with $n = 6$ and 7 corresponding to samples *am*PP6 and *am*PP7. These stress-relaxed fibers were stretched again at room temperature up to the break or up to a given elongation ϵ.

In the mechanical tests the ratio between the drawing rate and the initial length was fixed equal to 0.1 mm/(mm min) for the measurement of Young's modulus and 10 mm/(mm min) for the measurement of stress−strain curves and the determination of the other mechanical properties (stress and strain at the break and tension set). The values of the tension set were measured according to the standard test method ASTM D412-87. The specimens of initial length L_0 were stretched up to a length L_f, i.e., up to the elongation $\epsilon = [(L_f - L_0)/L_0] \times 100$, and held at this elongation for 10 min, then the tension was removed, and the final length of the relaxed specimens L_r was measured after 10 min. The tension set was calculated by using the formula $t_s(\epsilon) = [(L_r - L_0)/L_0] \times 100$, whereas the elastic recovery was calculated as $r(\epsilon) = [(L_f - L_r)/L_r] \times 100$. The reported values of the mechanical properties were averaged over at least five independent experiments.

The stress-relaxation tests were performed on unoriented compression-molded films following the procedure described in the standard test method ASTM D-2991-84. Instantaneous strains of 200% and 400% were applied, and the values of the stress were recorded as a function of time.

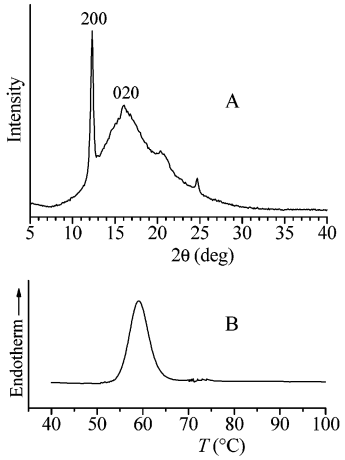

Figure 1. X-ray powder diffraction profile (A) and DSC curve recorded at a heating rate of 10 °C/min (B) of a compression-molded film of the *sam*PP1 sample. The film obtained by compression molding was kept at room temperature for one week to allow complete crystallization of the sample. The 200 and 020 reflections at $2\theta = 12.2°$ and 16°, respectively, of helical form I of s-PP are indicated.

Results and Discussion

Unoriented Films. As shown in ref 2, as-prepared *sam*-PP samples are amorphous and do not crystallize by cooling the melt to room temperature but slowly crystallize if the samples are kept at room temperature for several days. The *am*-PP samples, prepared with **3**/MAO, are instead fully amorphous and do not crystallize even for long aging time at room temperature. The X-ray powder diffraction profile and the DSC heating curve of a compression-molded film of the sample *sam*PP1, kept at room temperature for one week, are reported in Figure 1 as an example. *sam*-PP samples crystallize in disordered modifications of form I of s-PP, as indicated by the presence in the X-ray diffraction profile of Figure 1A of the 200 reflection at $2\theta = 12.2°$ and the broad halo centered on the 020 reflection at $2\theta = 16°$, typical of form I. Similar patterns are obtained for the other *sam*-PP samples. A maximum crystallinity of nearly 18−20% is achieved for the two more syndiotactic *sam*PP1 and *sam*PP2 samples ([*rrrr*] = 50−55%), with melting temperatures of 59 and 50 °C, respectively (Figure 1B). A lower crystallinity of nearly 16% is instead achieved for the less syndiotactic samples *sam*PP3, *sam*PP4, and *sam*PP5 ([*rrrr*] = 41−47%), regardless of the molecular weight, with melting temperatures of 47−48 °C.

Stress−strain curves of unoriented compression-molded films of crystalline *sam*-PP samples and amor-

Table 2. Elastic Modulus (E), Stress (σ_b) and Strain (ϵ_b) at the Break, Stress (σ_y) and Strain (ϵ_y) at the Yield Point, and Crystallinity (x_c) of Unoriented Compression-Molded Films of *sam*-PP and *am*-PP Samples[a]

sample	[*rrrr*] (%)	M_w	E (MPa)	σ_b (MPa)	ϵ_b (%)	σ_y (MPa)	ϵ_y (%)	x_c[b] (%)
s-PP	93	213000	256 ± 20	15 ± 1	400 ± 20	12 ± 1	10 ± 3	40
*sam*PP1	54.6	1308600	19 ± 4	7 ± 1	650 ± 60	3 ± 1	70 ± 5	20
*sam*PP2	51.6	672700	14 ± 2	6 ± 1	531 ± 67	3 ± 1	110 ± 10	18
*sam*PP3	45.8	1153200	4 ± 1	4 ± 1	630 ± 80	2.4 ± 0.4	90 ± 10	16
*sam*PP4	46.9	885700	1.2 ± 0.1	3 ± 1	580 ± 70	1.4 ± 0.2	82 ± 7	16
*sam*PP5	41.4	589200	4 ± 1	3.0 ± 0.5	430 ± 60	2.2 ± 0.4	90 ± 6	16
*am*PP6	26.5	1190800	0.5 ± 0.1	1.4 ± 0.1	880 ± 150	1.0 ± 0.1	130 ± 10	-
*am*PP7	25.7	385200	0.4 ± 0.1	-	-	0.5 ± 0.1	110 ± 10	-

[a] The fully syndiotactic pentad contents [*rrrr*] and the molecular weights (M_w) of the samples are also indicated. The data are compared with the mechanical properties of compression-molded films of the highly stereoregular and crystalline s-PP prepared with the C_s-symmetric metallocene catalyst.[20] [b] From X-ray powder diffraction profiles.

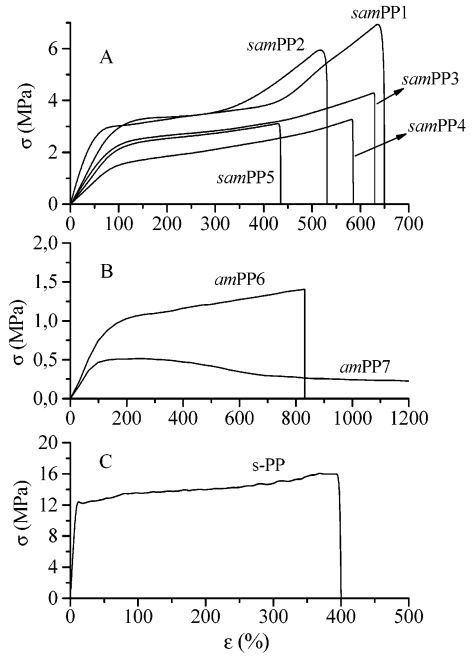

Figure 2. Stress−strain curves of unoriented compression-molded films of semicrystalline *sam*PP1−*sam*PP5 samples (A) and amorphous *am*PP6 and *am*PP7 samples (B). The stress−strain curve of a compression-molded film of highly stereoregular and crystalline s-PP prepared with a C_s-symmetric catalyst, taken from ref 20, is also reported for comparison (C).

phous *am*-PP samples, stretched at room temperature, are reported in Figure 2. These data are compared with the stress−strain curve of a compression-molded film of a highly stereoregular and crystalline s-PP sample, prepared with the classic C_s-symmetric metallocene catalyst, having a fully syndiotactic pentad content [*rrrr*] of 93%, taken from ref 20 (Figure 2C).

The mechanical properties (Young's modulus, stress and strain at the break, stress and strain at the yield point) and the values of the crystallinity of the starting compression-molded films of *sam*-PP and *am*-PP samples are reported in Table 2, and compared with the data for the highly stereoregular s-PP.

It is apparent from Figure 2 and Table 2 that, because of the lower crystallinity, the poorly syndiotactic *sam*-PP samples show values of the mechanical properties (stress at any strain, tensile strength, and Young's modulus) much lower than those of the highly stereoregular s-PP. The rigidity and the strength of semicrystalline polymeric materials are, indeed, an increasing function of the crystallinity. In particular, the values of Young's modulus are very high, 250−300 MPa, for the highly stereoregular and crystalline s-PP,[20] and decrease to about 10−20 MPa for *sam*PP1 and *sam*PP2 samples, 1−4 MPa for the lowest crystalline *sam*PP3−*sam*PP5 samples, and nearly 0.5 MPa for the amorphous *am*-PP samples. All the *sam*-PP samples show strains at the break higher than that observed for s-PP, indicating higher ductility according to the lower crystallinity. A comparison of *sam*-PP samples indicates a slight increase of the strain at the break with decreasing crystallinity and increasing molecular weight. Moreover, a higher tensile strength σ_b is observed for the more crystalline *sam*PP1 and *sam*PP2 samples. The amorphous *am*-PP samples show values of the strength much lower than those of the semicrystalline samples. In the case of sample *am*PP7, having the lowest molecular weight, high deformation without breaking and viscous flow for deformation higher than 500% are observed.

Table 3. Values of the Tension Set after Breaking (t_b) and the Tension Set ($t_s(\epsilon)$) and Elastic Recovery ($r(\epsilon)$) after Deformation ϵ for Unoriented Compression-Molded Films of *sam*-PP and *am*-PP Samples[a]

sample	t_s(200%) (%)	r(200%) (%)	t_s(400%) (%)	r(400%) (%)	t_b (%)
s-PP	-	-	300 ± 10	25 ± 3	300 ± 10
*sam*PP1	22 ± 6	146 ± 10	36 ± 1	268 ± 3	59 ± 8
*sam*PP2	20 ± 1	150 ± 2	31 ± 4	282 ± 12	48 ± 2
*sam*PP3	12 ± 1	167 ± 2	25 ± 1	300 ± 3	12 ± 2
*sam*PP4	12 ± 1	167 ± 2	25 ± 1	300 ± 3	13 ± 3
*sam*PP5	25 ± 1	140 ± 2	-	-	17 ± 6
*am*PP6	4 ± 1	188 ± 2	8 ± 2	363 ± 9	21 ± 8
*am*PP7	2 ± 1	194 ± 3	11 ± 2	350 ± 9	-

[a] Samples of initial length L_0 are stretched up to the break or up to strains ϵ of 200% and 400% (final lengths $L_f = 3L_0$ and $5L_0$), kept in tension for 10 min at room temperature, and then relaxed by releasing the tension. The data are compared with the mechanical properties of compression-molded films of the highly stereoregular and crystalline s-PP prepared with the C_s-symmetric metallocene catalyst.[20]

All the *sam*-PP samples show stress−strain curves typical of elastomers, with a small yield. Strain-hardening at high deformations, typical of elastomers, is observed mainly for the more stereoregular and crystalline *sam*PP1 and *sam*PP2 samples (Figure 2A and Table 1). The values of the tension set, $t_s(\epsilon) = [(L_r - L_0)/L_0] \times 100$, and the elastic recovery $r(\epsilon)$, measured at room temperature for unoriented films stretched up to deformations ϵ of 200% and 400%, or up to the break (t_b), are reported in Table 3.

These values were obtained by stretching the unoriented films of initial length L_0 up to the break, as in Figure 2, or up to a final length $L_f = 3L_0$ or $5L_0$ (for strains of 200% and 400%, respectively), keeping the specimens in tension for 10 min, then removing the

tension, and measuring the final length L_r of the relaxed sample after 10 min. The values of the tension set at the break and at 400% strain for unoriented films of highly crystalline s-PP are also reported in Table 3 for comparison.[20] The low values of the tension set of Table 3 indicate that all the *sam*-PP samples experience a recovery of the initial dimension either after breaking or after removal of the tension from a given deformation.

As reported in the literature,[20,21,26] unoriented films, not previously stretched, of highly stereoregular and crystalline s-PP samples, show poor elastic properties after the first stretching. The values of the tension set at the break, or after deformations higher than 400%, are indeed around 300% (Table 3).[20] In fact, unoriented compression-molded samples of s-PP behave like a typical highly crystalline material showing a plastic deformation upon stretching at room temperature.[20,21,25,26] The crystalline domains, with chains in a helical conformation, tend to assume a preferred orientation along the stretching direction, causing a plastic, not reversible, deformation. The poorly syndiotactic *sam*-PP samples show instead low values of the tension set, indicating good elastic properties at room temperature after the first stretching of unoriented films (Table 3). The more crystalline *sam*PP1 and *sam*PP2 samples present values of the tension set in the range 20−30%, for deformation lower than the strain at the break, which increase to values of nearly 50−60% when the samples are stretched up to the break. For the less stereoregular and crystalline samples *sam*PP3−*sam*PP5 values of the tension set of 20−25% are obtained, whereas amorphous *am*-PP samples show values of the tension set lower than 10%, indicating good elastic behavior (Table 3).

The amorphous sample *am*PP7 having the lowest molecular weight experiences a rapid viscous flow of the chains at deformations higher than 500% (Figure 2B) and/or by application of a constant stress. For this reason the very low values of the tension set were measured when the tension was removed soon after the deformation. This indicates that the sample shows elastic behavior only at low deformation and loses strength by application of stresses for a long time. Therefore, for amorphous *am*-PP samples prepared with the Dow catalyst **3**/MAO, only when the molecular weight is very high (sample *am*PP6) is the viscous flow prevented, giving interesting elastic properties but, however, with very low strength. The presence of crystallinity in the *sam*-PP samples, prepared with **1**/MAO and **2**/MAO, increases the values of the modulus and the stress at any strain, producing interesting thermoplastic elastomers with higher strength.

However, since the melting temperatures of the crystalline *sam*-PP samples are rather low (in the range 47−60 °C, Table 1) and the onset of the melting is around 55 °C for the more stereoregular samples (Figure 1B) and 40 °C for the less stereoregular samples, it is worth emphasizing that the described outstanding mechanical properties are valid at room temperature (25−40 °C). At higher temperatures a behavior similar to that of the high-molecular-weight amorphous *am*PP6 sample is expected.

As shown in Figure 1, all the unoriented films of *sam*-PP samples, used for the mechanical tests, are always in a disordered modification of helical form I, as generally occurs also in films prepared by compression molding of highly stereoregular and crystalline s-PP samples.[14,20] Moreover, the structural analysis reported in our previous paper[2] indicates that in these samples helical form I transforms by stretching into the disordered mesomorphic *trans*-planar form. This is shown as an example in Figure 3A,A′, where the X-ray fiber diffraction pattern, and the corresponding profile read along the equatorial line, of a fiber of sample *sam*PP1 obtained by stretching compression-molded films up to 400% elongation is reported.

The presence of the broad equatorial reflection at $2\theta \approx 17°$, typical of the *trans*-planar mesomorphic form, is apparent (Figure 3A). Only a small amount of helical form I is still present, as indicated by the presence of the 200 reflection at $2\theta = 12°$ of low intensity (Figure 3A′). We recall that, for the highly stereoregular s-PP, helical form I transforms instead into *trans*-planar form III by stretching.[12,15,20]

The X-ray diffraction pattern, and the corresponding profile read along the equatorial line, of the fiber of Figure 3A after the tension was removed is shown in Figure 3B,B′. It is apparent that the mesomorphic form transforms into helical form I upon release of the tension, as indicated by the presence of the 200 and 020 reflections at $2\theta = 12°$ and 16° in the pattern of Figure 3B,B′.[2] In the case of the highly stereoregular s-PP, *trans*-planar form III, obtained by stretching, transforms instead into isochiral form II upon release of the tension.[15,20,21]

These data suggest that the different elastic behaviors of highly stereoregular s-PP and poorly syndiotactic *sam*-PP samples are basically related to the different crystallinities, and indicate that the chains in the amorphous phase play an important role in the elastic recovery. Highly stereoregular s-PP samples, with fully syndiotactic pentad content [*rrrr*] higher than 70−80%, not previously stretched, show poor elastic properties when stretched for the first time because of the occurrence of the irreversible plastic deformation due to the high crystallinity. Low-stereoregular *sam*-PP samples, with fully syndiotactic pentad content [*rrrr*] around 50%, show good elastic properties at room temperature even during the first stretching and do not experience irreversible plastic deformation because of the very low crystallinity. The small crystalline domains in the amorphous matrix act as physical knots of the elastomeric lattice, preventing the viscous flow of the amorphous chains and giving rise to a typical thermoplastic elastomeric behavior, where the entropic effect of the conformational transition of the amorphous chains is mainly responsible for the elasticity. The chains belonging to the amorphous phase, connecting the crystalline regions, undergo a reversible conformational transition between the entropically favored disordered random coil conformation in the unstretched state and the extended conformation in the stretched state. Since the molecular weights of *sam*-PP samples are very high, these amorphous chains are highly entangled and connect, as tie chains, the small crystalline domains. They act as springs between the crystals, being well-oriented and in an extended conformation in the stretched state, and returning to the disordered coil conformation when the tension is removed.

Moreover, since the small crystalline domains are characterized by a disordered modification (disordered form I), which transforms into the disordered mesomorphic form, they can be more easily plastically deformed. It is well-known, indeed, that mesomorphic crystalline

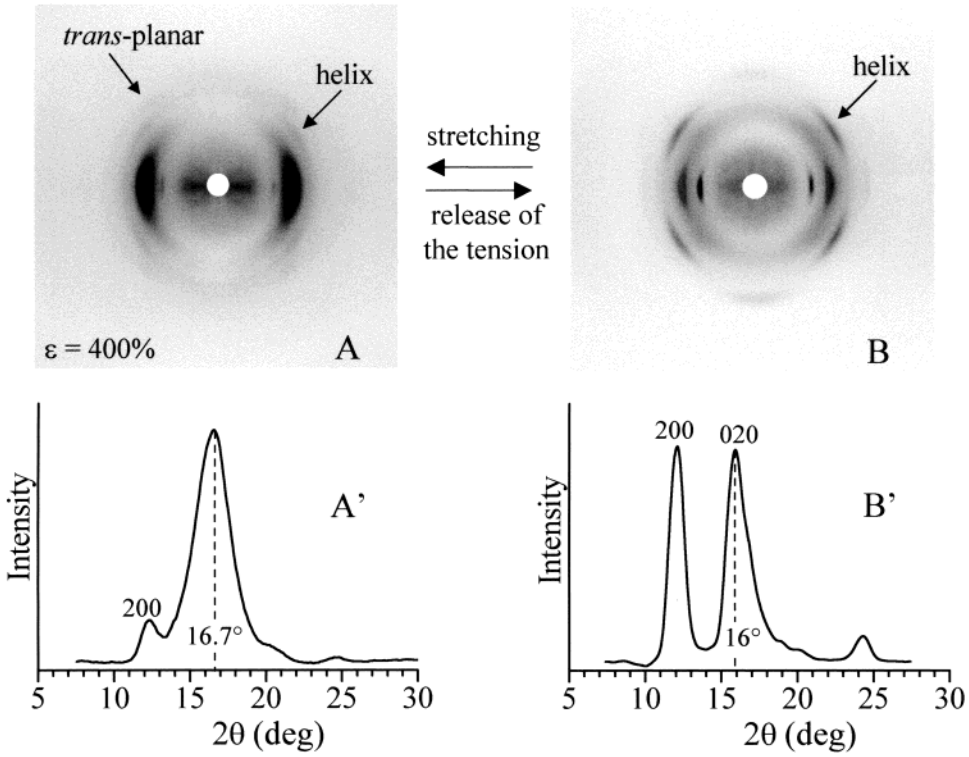

Figure 3. X-ray fiber diffraction patterns, after the subtraction of the amorphous halo (A, B), and corresponding profiles read along the equatorial lines (A′, B′), of fibers of sample *sam*PP1 obtained by stretching compression-molded films at 400% elongation, while the fiber was kept under tension (A) and after the tension was removed (B). The 200 and 020 reflections at $2\theta = 12.2°$ and 16°, respectively, typical of helical form I of s-PP, and the broad reflection of the mesomorphic form at $2\theta = 16.7°$, are indicated. The fiber in (A) is in the *trans*-planar mesomorphic form with a small amount of the helical form, whereas the fiber in (B) is basically in helical form I.

phases, characterized by a high degree of structural disorder, present better deformation properties than the ordered crystalline forms. Finally, along with these effects, an enthalpic contribution due to the structural transition from the mesomorphic form into helical form I (Figure 3) occurring in the small crystalline domains assists the elastic recovery of the samples.

In the case of the amorphous *am*-PP samples, the high molecular weight, which guarantees a high degree of entanglement of the chains, is responsible for the elastic recovery but, in the case of sample *am*PP7, is not sufficient to prevent the viscous flow at high deformations.

Oriented Fibers. The mechanical analysis was also performed on oriented stress-relaxed fibers of the semicrystalline *sam*-PP and amorphous *am*-PP samples. These stress-relaxed fibers were prepared by stretching compression-molded films of *sam*-PP and *am*-PP samples of initial length L_0 up to 200% and 400% elongation (the final length L_f being $3L_0$ and $5L_0$, respectively), keeping the fibers under tension for 10 min at room temperature, and then removing the tension (the fibers stress-relaxed from 200% and 400% elongations are identified as *sam*PP*n*-200, *sam*PP*n*-400, *am*PP*n*-200, and *am*PP*n*-400, with n =1−5 corresponding to samples *sam*PP1−*sam*PP5 of Table 1 and n = 6 and 7 corresponding to samples *am*PP6 and *am*PP7). After the relaxation, the final length of these fibers is $L_r = L_0(t_s/100) + L_0$, where t_s is the value of the tension set reported in Table 3.

As discussed above and shown in Figure 3 for sample *sam*PP1, stress-relaxed fibers of *sam*-PP samples are in helical form I.[2] The mesomorphic form, obtained by stretching at $\epsilon = 400\%$ (Figure 3A), transforms, indeed, into helical form I by removal of the tension, as indicated by the presence of the strong 200 and 020 reflections at $2\theta = 12.2°$ and 16°, respectively, in the pattern of Figure 3B,B′.

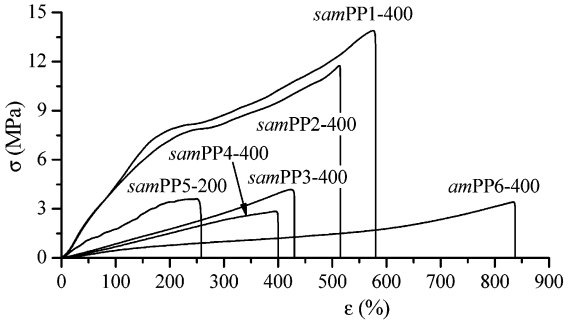

Figure 4. Stress−strain curves of strained and stress-relaxed fibers *sam*PP*n*-400 (n = 1−4) and *am*PP6-400. Stress-relaxed fibers *sam*PP*n*-400 and *am*PP*n*-400 are obtained by stretching compression-molded films of *sam*-PP and *am*-PP samples up to 400% elongation, keeping the fiber under tension for 10 min at room temperature, and then removing the tension. For sample *sam*PP5 the stress−strain curve of the *sam*PP5-200 fibers, stress-relaxed from 200% elongation, is reported.

The stress−strain curves of the stress-relaxed fibers *sam*PP*n*-400 and *am*PP*n*-400 are reported in Figure 4. The mechanical properties of the fibers are reported in Table 4. In the case of sample *sam*PP5, fibers stress-relaxed from 400% elongation could not be prepared because the sample breaks at nearly $\epsilon = 400\%$ (Table 2), and only the stress−strain curve of the fiber *sam*PP5-200 is reported in Figure 4.

It is apparent from Figure 4 and Table 4 that, for fibers of the more stereoregular samples *sam*PP1 and *sam*PP2, the values of the stress at a given elongation,

Table 4. Elastic Modulus (E), Stress (σ_b), Strain (ϵ_b), and Tension Set (t_b) at the Break, and Tension Set ($t_s(\epsilon)$) and Elastic Recovery ($r(\epsilon)$) at the Elongation ϵ (%) for Strained and Stress-Relaxed Fibers of *sam*-PP and *am*-PP Samples[a]

sample	E (MPa)	σ_b (MPa)	ϵ_b (%)	t_b (%)	$t_s(\epsilon)^b$ (%)	$r(\epsilon)^b$ (%)
sPP-400	335 ± 20	30 ± 2	25 ± 5	0	0	25
*sam*PP1-400	5 ± 1	15 ± 3	580 ± 111	54 ± 8	15	220
*sam*PP2-400	2 ± 1	12 ± 2	515 ± 76	69 ± 4	23	211
*sam*PP3-400	1.0 ± 0.6	4.0 ± 0.7	430 ± 100	12 ± 1	8.5	269
*sam*PP4-400	0.54 ± 0.02	2.8 ± 0.2	400 ± 50	12 ± 1	5.0	281
*sam*PP5-200	1.6 ± 0.3	3.6 ± 0.4	258 ± 10	10 ± 1	0	140
*am*PP6-400	0.1 ± 0.1	3.4 ± 0.8	837 ± 60	2.6 ± 0.6	3.8	346

[a] The stress-relaxed fibers *sam*PP*n*-400 with $n = 1-4$ and *am*PP6-400 were obtained by stretching compression-molded films of *sam*PP1−*sam*PP4 and *am*PP6 samples, respectively, up to 400% elongation, keeping the fiber under tension for 10 min at room temperature, and then removing the tension. For sample *sam*PP5 only the values of the fiber *sam*PP5-200, stress-relaxed from 200% strain, are reported because the sample breaks at 400% elongation. The data are compared with the mechanical properties of stress-relaxed fibers of the highly stereoregular and crystalline s-PP prepared with the C_s-symmetric metallocene catalyst.[20] [b] The tension set $t_s(\epsilon)$ and the elastic recovery $r(\epsilon)$ were evaluated by stretching the fibers of initial length L_r up to the final length $L_f = 5L_0$, that is, up to the elongation $\epsilon = [(5L_0 - L_r)/L_r] \times 100$. $t_s(\epsilon) = [(L_r' - L_r)/L_r] \times 100$ and $r(\epsilon) = [(5L_0 - L_r')/L_r'] \times 100$, where L_r' is the final length after release of the tension.

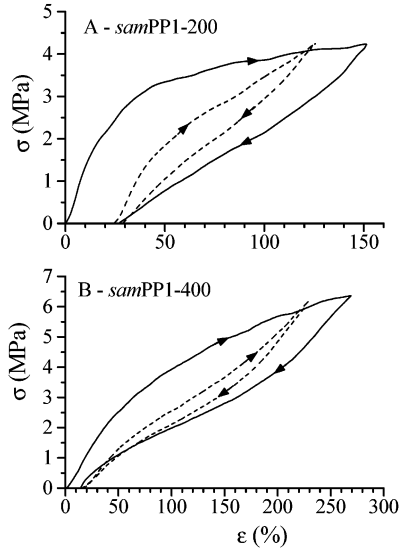

Figure 5. Stress−strain hysteresis cycles recorded at room temperature, composed of the stretching and relaxation (at a controlled rate) steps according to the direction of the arrows, for strained and stress-relaxed fibers of the *sam*-PP1 sample. *sam*PP1-200 (A) and *sam*PP1-400 (B) fibers are stress-relaxed from fibers stretched up to 200% and 400% elongation, respectively. In the hysteresis cycles the stretching steps are performed by stretching the fibers up to the final length $L_f = 3L_0$ (A) and $5L_0$ (B). The first hysteresis cycle (continuous lines) and curves averaged for at least four cycles successive to the first one (dashed lines) are reported.

as well as the stress at the break, are higher than those measured for unoriented films (Figure 2 and Table 2), whereas the values of the elongation at the break and the tension set at the break are nearly the same as those observed for the unoriented films. This indicates that the oriented fibers show good elastic behavior at room temperature with values of strength higher than those of the unoriented films. The values of the mechanical properties of fibers of the less crystalline samples *sam*PP3−*sam*PP5 are basically the same as observed for unoriented samples (Tables 2 and 4).

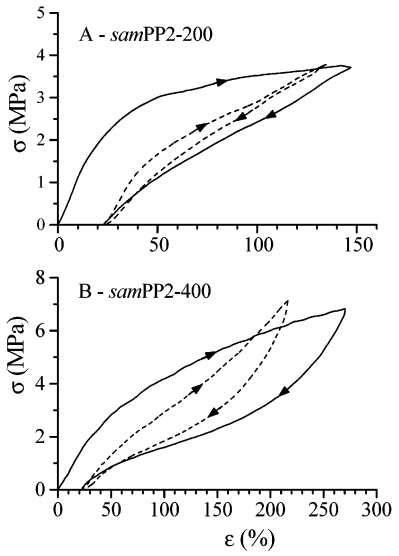

Figure 6. Stress−strain hysteresis cycles recorded at room temperature, composed of the stretching and relaxation (at a controlled rate) steps according to the direction of the arrows, for strained and stress-relaxed fibers of the *sam*-PP2 sample. *sam*PP2-200 (A) and *sam*PP2-400 (B) fibers are stress-relaxed from fibers stretched up to 200% and 400% elongation, respectively. In the hysteresis cycles the stretching steps are performed by stretching the fibers up to the final length $L_f = 3L_0$ (A) and $5L_0$ (B). The first hysteresis cycle (continuous lines) and curves averaged for at least four cycles successive to the first one (dashed lines) are reported.

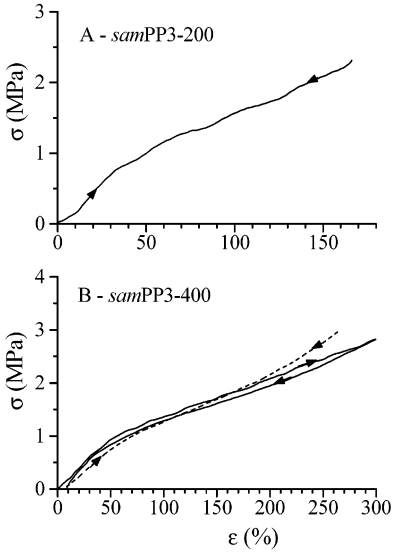

Figure 7. Stress−strain hysteresis cycles recorded at room temperature, composed of the stretching and relaxation (at a controlled rate) steps according to the direction of the arrows, for strained and stress-relaxed fibers of the *sam*-PP3 sample. *sam*PP3-200 (A) and *sam*PP3-400 (B) fibers are stress-relaxed from fibers stretched up to 200% and 400% elongation, respectively. In the hysteresis cycles the stretching steps are performed by stretching the fibers up to the final length $L_f = 3L_0$ (A) and $5L_0$ (B). The first hysteresis cycle (continuous lines) and curves averaged for at least four cycles successive to the first one (dashed lines) are reported.

The high-molecular-weight amorphous sample *am*PP6 presents instead tensile strength and modulus lower than those of the unstretched films probably because the first stretching induces remarkable disentanglement of the chains. In the case of the amorphous sample *am*PP7 with lower molecular weight, even though the unoriented film shows good elastic properties during the

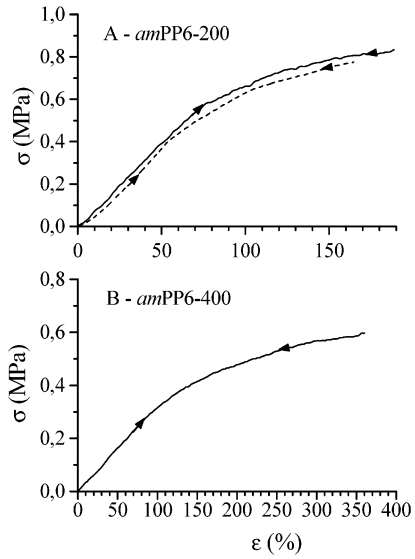

Figure 8. Stress−strain hysteresis cycles recorded at room temperature, composed of the stretching and relaxation (at a controlled rate) steps according to the direction of the arrows, for strained and stress-relaxed fibers of the *am*-PP6 sample. *am*PP6-200 (A) and *am*PP6-400 (B) fibers are stress-relaxed from fibers stretched up to 200% and 400% elongation, respectively. In the hysteresis cycles the stretching steps are performed by stretching the fibers up to the final length $L_f = 3L_0$ (A) and $5L_0$ (B). The first hysteresis cycle (continuous lines) and curves averaged for at least four cycles successive to the first one (dashed lines) are reported.

first stretching at low deformation, the viscous flow observed at higher deformation (Figure 2B) prevents the performance of mechanical tests after the first stretching.

The values of the tension set $t_s(\epsilon)$ and the elastic recovery $r(\epsilon)$ of oriented *sam*PP*n*-400 fibers, stress-relaxed from 400% elongation, are also reported in Table 4. These values were measured by stretching at room temperature fibers relaxed from 400% elongation, having the new initial length L_r, up to the final length $L_f = 5L_0$, that is, up to an elongation $\epsilon = [(L_f - L_r)/L_r] \times 100$ (corresponding to the elastic recovery reported in Table 3, i.e., $\epsilon = 268\%$, 282%, 300%, and 300% for the *sam*PP1-400, *sam*PP2-400, *sam*PP3-400, and *sam*PP4-400 fibers, respectively), keeping the fibers in tension for 10 min, then removing the tension, and measuring the final length of the relaxed fibers after 10 min. These values of the elongation ϵ were chosen to reduce the possibility of new plastic deformation of the fibers during the measure of the elastic recovery. In the case of sample *sam*PP5, the value of the tension set for the stress-relaxed fiber *sam*PP5-200, stretched up to $L_f = 3L_0$, is reported in Table 4. The low values of the tension set (Table 4), and the shape of the stress−strain curves of Figure 4, indicate that the stress-relaxed fibers show good elastic behavior.

To quantify the elastic properties of fibers of *sam*-PP and *am*-PP samples, hysteresis cycles were performed at room temperature on the oriented stress-relaxed fibers. The hysteresis cycles, composed of the stress−strain curves measured during the stretching, immediately followed by the curves measured during the relaxation at a controlled rate, are reported in Figures 5−7 for the crystalline *sam*PP*n*-200 and *sam*PP*n*-400 fibers, and in Figure 8 for the amorphous *am*PP6-200 and *am*PP6-400 samples. In these cycles, stress-relaxed oriented fibers of the new initial length L_r are stretched up to the final length $L_f = 3L_0$ for fibers *sam*PP*n*-200 and *am*PP6-200, or $L_f = 5L_0$ for fibers *sam*PP*n*-400 and *am*PP6-400, that is, up to a maximum strain $\epsilon_{max} = [(L_f - L_r)/L_r] \times 100$, numerically coincident with the elastic recovery reported in Table 3. As discussed before, this choice of the maximum strain in the hysteresis cycles is due to the need to reduce to a minimum a new plastic deformation of the fibers during the stretching step of the hysteresis cycles.

For each fiber, four successive cycles were recorded; each cycle was performed 10 min after the end of the previous cycle. Successive hysteresis cycles, measured after the first one, are all nearly coincident, indicating a tension set close to zero. All the stress-relaxed fibers recover almost completely the initial dimensions. The values of the residual tension set and the percent of dissipated energy (hysteresis), measured after each cycle, are reported in Table 5. In the case of fibers of semicrystalline and more stereoregular *sam*PP1 and *sam*PP2 samples, the residual tension set between the first and second hysteresis cycles is around 20% and becomes close to zero starting from the second cycle, the successive cycles, measured after the first one, being all nearly coincident. The dissipated energy is nearly 50% during the first cycle and is reduced to 10−20% in the successive cycles. For fibers of the lower crystalline samples *sam*PP3−*sam*PP5, the values of the tension set are nearly zero in all hysteresis cycles performed at low deformations, and increase to 5−10% after the first cycle at higher deformation (Table 5). In the case of the high-molecular-weight amorphous sample *am*PP6, the values of the tension set and of the hysteresis are nearly zero in all cycles.

These data indicate that both unoriented films and oriented fibers of the low-stereoregular nearly amorphous *sam*-PP samples present good elastic properties in a large range of deformation.

It is worth noting that the most important difference in the elastic behavior of highly stereoregular and crystalline s-PP[20,21] is the different ranges of deformability. In fact, as discussed above, when oriented fibers of highly stereoregular s-PP are prepared by stretching compression-molded films, only a small recovery of the initial dimension occurs upon release of the tension, because of the occurrence of the irreversible plastic deformation of the highly crystalline materials (see Table 2).[20,21] For this reason the range of deformation within which highly stereoregular s-PP fibers can be used as elastomers, between the new length of oriented fibers and the maximum achievable elongation, is very small (about 60−65% strain).[20,21] In the case of the low-stereoregular *sam*-PP samples instead, since the stretched unoriented films experience a nearly total recovery of the initial dimension upon removal of the tension, the tension set observed after the first stretching being very low even for large deformation ($t_s(200\%) = 10-25\%$ and $t_s(400\%) = 20-36\%$; see Table 3), the oriented fibers can be used as elastomers in a large range of deformation, up to the maximum deformation achieved during the preparation of the fibers.

As discussed above, in the small crystalline domains of *sam*-PP samples a polymorphic reversible transition between helical form I and the *trans*-planar mesomorphic form occurs by stretching unoriented films and removing the tension (Figure 3). This reversible transition occurs also in the stress-relaxed oriented fibers upon successive stretching and relaxing cycles, as in the

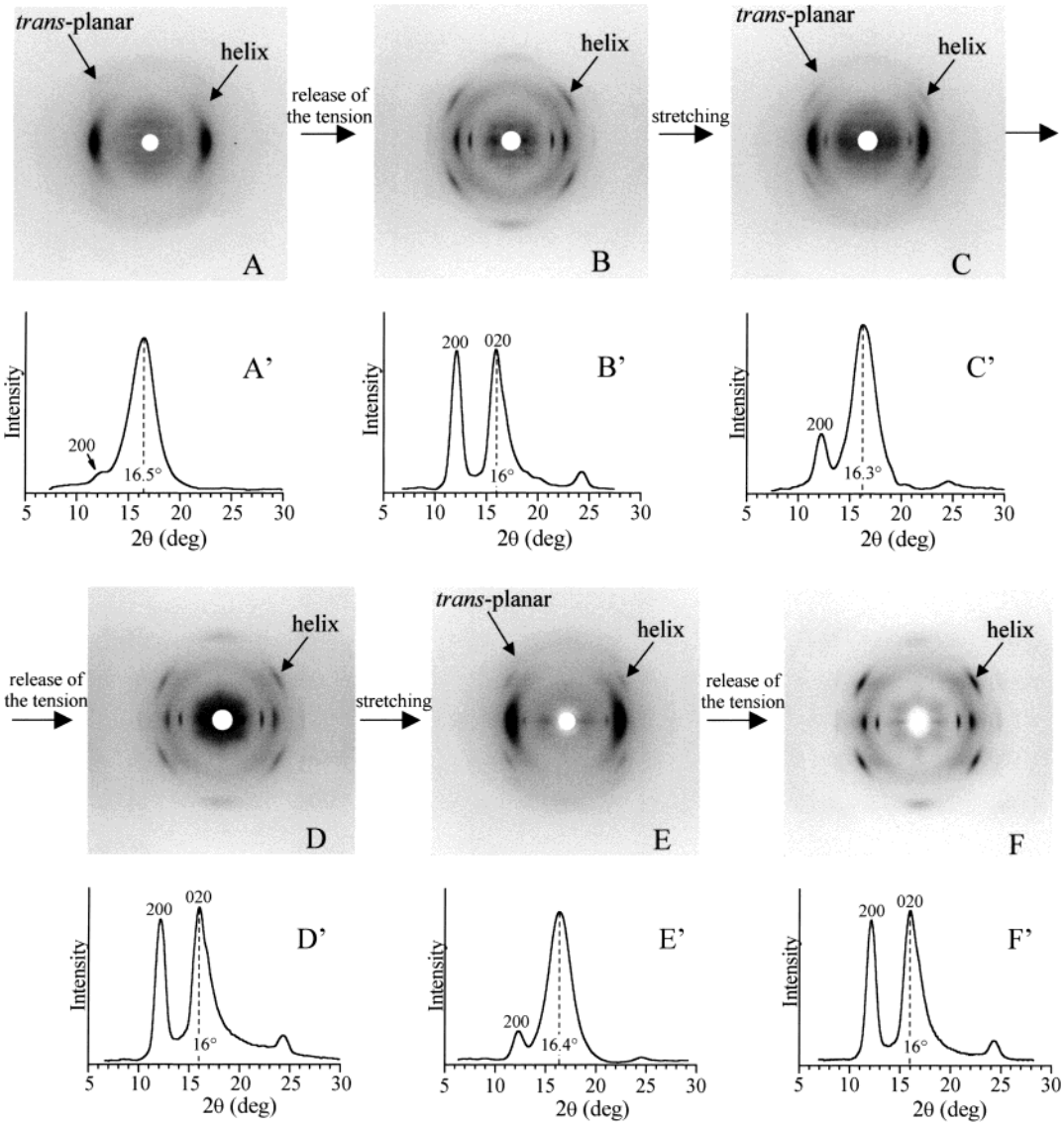

Figure 9. X-ray fiber diffraction patterns, after the subtraction of the amorphous halo (A−F), and corresponding profiles read along the equatorial lines (A′−F′), of the stress-relaxed *sam*PP1-400 fiber of sample *sam*PP1 during three successive stretching−relaxing cycles. The stress-relaxed fiber *sam*PP1-400 was obtained by stretching compression-molded films up to 400% elongation and then removing the tension. The *sam*PP1-400 fiber was stretched up to the maximum elongation $L_f = 5L_0$ achieved in the first hysteresis cycle of Figure 5, and the diffraction patterns were recorded while the fiber was kept in tension (A), after the tension was removed (B), after the fiber was stretched again up to $L_f = 5L_0$ in the second cycle (C), after the tension was removed (D), after the fiber was stretched again up $L_f = 5L_0$ in the third cycle (E), and after the tension was removed (F). The 200 and 020 reflections at $2\theta = 12.2°$ and 16°, respectively, typical of helical form I of s-PP, and the broad reflection of the mesomorphic form at $2\theta = 16-17°$, are indicated.

Table 5. Values of the Tension Set (t_s) and the Dissipated Energy (E_{diss}) Measured in the Four Hysteresis Cycles of Figures 5−8 for Stress-Relaxed Fibers of *sam*-PP and *am*-PP Samples

sample	t_s (%) (cycle I)	t_s (%) (cycle II)	t_s (%) (cycles III and IV)	E_{diss} (%) (cycle I)	$\langle E_{diss} \rangle$ (%) (cycles II−IV)
*sam*PP1-200	24.8	2.3	0	52	21
*sam*PP1-400	15	0.4	0	35	10
*sam*PP2-200	22.8	2.3	0	42	9
*sam*PP2-400	22.7	2.4	0	47	26
*sam*PP3-200	0	0	0	0	0
*sam*PP3-400	8.5	1.6	0	5.5	0.4
*sam*PP4-200	0	0	0	0	0
*sam*PP4-400	5	0	0	3.1	0.6
*sam*PP5-200	0	0	0	0	0
*am*PP6-200	1.3	0	0	0	0
*am*PP6-400	3.8	0	0	0	0

hysteresis cycles of Figures 5−7. This is shown in Figure 9, which reports the X-ray fiber diffraction patterns, and the corresponding equatorial profiles, of the fiber *sam*PP1-400 stretched and relaxed in three successive hysteresis cycles.

The comparison with the diffraction patterns obtained in the first stretching of the unoriented film of the same sample of Figure 3 indicates that a higher degree of orientation of the crystals of both the *trans*-planar mesomorphic form and helical form I is achieved

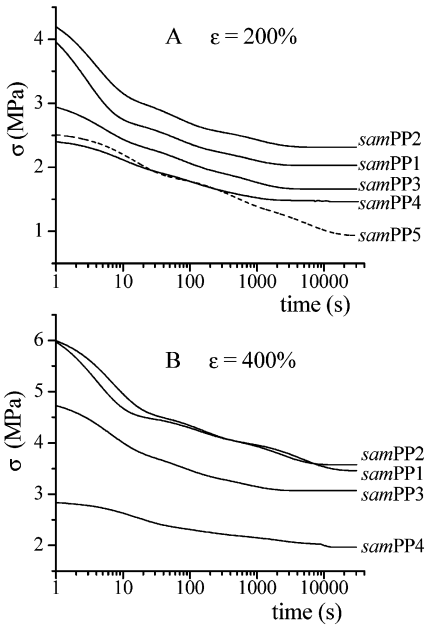

Figure 10. Stress-relaxation curves of *sam*-PP samples. The values of the stress are reported as a function of time for compression-molded films after application of instantaneous strains of 200% (A) and 400% (B).

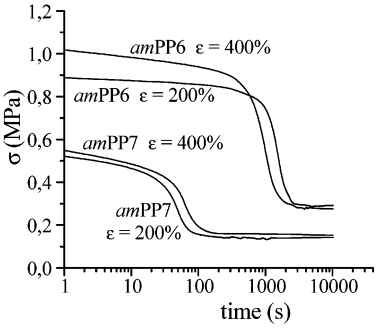

Figure 11. Stress-relaxation curves for amorphous *am*PP6 and *am*PP7 samples. The values of the stress are reported as a function of time for compression-molded films after application of instantaneous strains of 200% and 400%.

through the successive stretching−relaxing cycles. The energy dissipated during the first hysteresis cycle (Figure 5) is likely related to this morphological transformation. This makes the hysteresis in the first cycle higher than that in the successive cycles.

Stress-Relaxation Tests for Unoriented Films. Stress-relaxation experiments were performed at room temperature on the compression-molded films of *sam*-PP and *am*-PP samples to test the strength of these materials in conditions of deformation for a long time. The values of the stress were recorded as a function of the time after application on compression-molded films of instantaneous strains of 200% and 400%. The stress-relaxation curves of compression-molded films of the semicrystalline *sam*-PP samples and of the amorphous *am*-PP samples are reported in Figures 10 and 11, respectively.

The samples show a typical behavior of viscoelastic materials. For the semicrystalline *sam*PP1, *sam*PP2, *sam*PP3, and *sam*PP4, a small loss of the stress of 35−40% after nearly 300 s, regardless of the instantaneous deformation, is observed. Then the stress remains constant at values as high as 2−4 MPa for a long time. For the amorphous *am*-PP samples (Figure 11) a higher loss of the stress, of about 70%, is observed after 1000 s for sample *am*PP6 having a high molecular weight, and only 70 s for sample *am*PP7 with lower molecular weight. These data confirm the previous observations that semicrystalline *sam*-PP samples behave at room temperature as elastomers in a large deformation range and show high toughness and ductility and remarkable strength even when stresses are applied for a long time. Amorphous samples show instead a higher loss of strength in a short time; moreover, the lowest molecular weight *am*PP7 sample presents good elastic behavior only in the first stretching and loses strength in a few seconds.

Conclusions

The analysis of the mechanical properties of the poorly syndiotactic *sam*-PP samples, prepared with catalysts **1**/MAO and **2**/MAO, has shown that these materials present values of the stress at any strain, tensile strength, and Young's modulus much lower than those of the highly stereoregular and crystalline s-PP, as a consequence of the lower crystallinity. All the *sam*-PP samples show strains at the break higher than that observed for s-PP, indicating higher ductility according to the lower crystallinity.

The comparison with the amorphous *am*-PP samples, prepared with the Dow catalyst **3**/MAO, shows that the amorphous samples present a lower strength and experience rapid viscous flow of the chains at high deformations and/or by application of stresses for a long time.

The semicrystalline low stereoregular *sam*-PP samples show good elastic behavior at room temperature. For the amorphous *am*-PP samples, instead, only when the molecular weight is very high (sample *am*PP6) is the viscous flow prevented, giving interesting elastic properties but, however, with very low strength. The presence of crystallinity in *sam*-PP samples increases the values of the modulus and the stress at any strain, producing interesting thermoplastic elastomeric materials with higher strength.

For the semicrystalline *sam*-PP samples the elastic behavior is associated with a reversible polymorphic transition between the *trans*-planar mesomorphic form and helical form I, which occurs during successive stretching and relaxing of fiber specimens. The *trans*-planar mesomorphic form is stable only in the stretched state and transforms into the more stable helical form I upon release of the tension. The same behavior was revealed in the highly stereoregular and crystalline s-PP sample,[20,21] with the difference that the reversible polymorphic transition occurs between *trans*-planar form III and helical form II of s-PP.

Remarkable differences in the elastic properties of highly stereoregular and crystalline s-PP and low-stereoregular *sam*-PP samples have been found. Unoriented films of s-PP show poor elastic properties after the first stretching because of the occurrence of the irreversible plastic deformation, typical of highly crystalline materials. Only oriented fibers of s-PP present good elastic behavior in a small range of deformation. The low-stereoregular and crystalline *sam*-PP samples present good elastic properties at room temperature not only for oriented fibers but also during the first stretching of unoriented compression-molded films. Because of the very low crystallinity, these materials experience a negligible plastic deformation and show a typical thermoplastic elastomeric behavior. The small crystalline

domains in the amorphous matrix act as physical knots of the elastomeric lattice, preventing the viscous flow of the amorphous chains. The entropic effect of the conformational transition of the amorphous chains is mainly responsible for the elasticity. Since the molecular weights of the samples are very high, these amorphous chains are highly entangled and connect as tie chains the small crystalline domains. They act as springs between the crystals, being well-oriented and in an extended conformation in the stretched state, and returning to the disordered coil conformation when the tension is removed. Moreover, since the small crystalline domains are characterized by a disordered modification (disordered form I), which transforms into the disordered mesomorphic form, they can be more easily plastically deformed. Finally, along with these effects, an enthalpic contribution due to the structural transition from the mesomorphic form into helical form I assists the elastic recovery of the samples.

Since the stretched unoriented films of *sam*-PP samples experience a nearly total recovery of the initial dimension upon removal of the tension, the corresponding oriented fibers behave at room temperature (25−40 °C) as elastomers in a large range of deformation, up to the maximum deformation achieved during the preparation of the fibers. They also show high toughness and ductility and remarkable strength even when stresses are applied for a long time.

Acknowledgment. Financial support from Basell Polyolefins (Ferrara, Italy) and from the "Ministero dell'Istruzione, Università e Ricerca Scientifica" (PRIN 2002 and Cluster C26 projects) is gratefully acknowledged. We thank Dr. Luigi Resconi of Basell for having stimulated this study and providing polymer samples having a desired microstructure, giving a unique opportunity to study the relationships between molecular structure and mechanical properties.

References and Notes

(1) De Rosa, C.; Auriemma, F.; Ruiz de Ballesteros, O.; Resconi, L.; Fait, A.; Ciaccia, E.; Camurati, I. *J. Am. Chem. Soc.* **2003**, *125*, 10913.
(2) De Rosa, C.; Auriemma, F.; Ruiz de Ballesteros, O. *Macromolecules* submitted.
(3) Resconi, L.; Guidotti, S.; Baruzzi, G.; Grandini, C.; Nifant'ev, I. E.; Kashulin, I. A.; Ivchenko, P. V. PCT Int. Appl. WO 01/53360, 2001. Basell, Italy. Grandini, C.; Camurati, I.; Guidotti, S.; Mascellari, N.; Resconi, L.; Nifant'ev, I. E.; Kashulin, I. A.; Ivchenko, P. V.; Mercandelli, P.; Sironi, A. *Organometallics*, submitted for publication.
(4) Stevens, J. C.; Timmers, F. J.; Wilson, D. R.; Schmidt, G. F.; Nickias, P. N.; Rosen, R. K.; Knight, G. W.; Lai, S. Y. (Dow Chemical Co.). Eur. Pat. Appl. 0 416 815, 1990.
(5) Corradini, P.; Natta, G.; Ganis, P.; Temussi, P. A. *J. Polym. Sci., Part C: Polym. Lett.* **1967**, *16*, 2477.
(6) Lotz, B.; Lovinger, A. J.; Cais, R. E. *Macromolecules* **1988**, *21*, 2375.
(7) Lovinger, A. J.; Lotz, B.; Davis, D. D. *Polymer* **1990**, *31*, 2253.
(8) Lovinger, A. J.; Davis, D. D.; Lotz, B. *Macromolecules* **1991**, *24*, 552
(9) Lovinger, A. J.; Lotz, B.; Davis, D. D.; Padden, F. J. *Macromolecules* **1993**, *26*, 3494.
(10) Chatani, Y.; Maruyama, H.; Noguchi, K.; Asanuma, T.; Shiomura, T. *J. Polym. Sci., Part C: Polym. Lett.* **1990**, *28*, 393.
(11) Chatani, Y.; Maruyama, H.; Asanuma, T.; Shiomura, T. *J. Polym. Sci., Part B: Polym. Phys.* **1991**, *29*, 1649.
(12) De Rosa, C.; Corradini, P. *Macromolecules* **1993**, *26*, 5711.
(13) De Rosa, C.; Auriemma, F.; Corradini, P. *Macromolecules* **1996**, *29*, 7452.
(14) De Rosa, C.; Auriemma, F.; Vinti, V. *Macromolecules* **1997**, *30*, 4137.
(15) De Rosa, C.; Auriemma, F.; Vinti, V. *Macromolecules* **1998**, *31*, 7430.
(16) De Rosa, C.; Auriemma, F.; Vinti, V.; Galimberti, M. *Macromolecules* **1998**, *31*, 6206.
(17) Auriemma, F.; De Rosa, C.; Ruiz de Ballesteros, O.; Vinti, V. *J. Polym. Sci., Part B: Polym. Phys.* **1998**, *36*, 395.
(18) Nakaoki, T.; Ohira, Y.; Hayashi, H.; Horii, F. *Macromolecules* **1998**, *31*, 2705.
(19) Vittoria, V.; Guadagno, L.; Comotti, A.; Simonutti, R.; Auriemma, F.; De Rosa, C. *Macromolecules* **2000**, *33*, 6200.
(20) Auriemma, F.; Ruiz de Ballesteros, O.; De Rosa, C. *Macromolecules* **2001**, *34*, 4485.
(21) De Rosa, C.; Gargiulo, M. C.; Auriemma, F.; Ruiz de Ballesteros, O.; Razavi, A. *Macromolecules* **2002**, *35*, 9083.
(22) De Rosa, C.; Auriemma, F.; Ruiz de Ballesteros, O. *Polymer* **2001**, *42*, 9729.
(23) De Rosa, C.; Auriemma, F.; Orlando, I.; Talarico, G.; Caporaso, L. *Macromolecules* **2001**, *34*, 1663.
(24) Lotz, B.; Mathieu, C.; Thierry, A.; Lovinger, A. J.; De Rosa, C.; Ruiz de Ballesteros, O.; Auriemma, F. *Macromolecules* **1998**, *31*, 9253.
(25) Loos, J.; Schimanki, T. *Polym. Eng. Sci.* **2000**, *40*, 567.
(26) D'Aniello, C.; Guadagno, L.; Naddeo, C.; Vittoria, V. *Macromol. Chem., Rapid Commun.* **2001**, *22*, 104. Guadagno, L.; D'Aniello, C.; Naddeo, C.; Vittoria, V. *Macromolecules* **2001**, *34*, 2512. Guadagno, L.; D'Aniello, C.; Naddeo, C.; Vittoria, V.; Meille, S. V. *Macromolecules* **2002**, *35*, 3921.

MA034829K